Supplementary Information

Network edges at the tRNA·GluRS interface

The total number of contacts decreases in the post-transfer states, primarily around the acceptor stem and CCA hairpin. Notable exceptions occur in the Post (no AMP) and Post (no AMP/GluNH$_2$) states. The tRNA in the Post (no AMP) state maintains a high number of contacts between the CCA hairpin and GluRS. In particular, C74 undergoes a slight conformational change in the other simulations, which only occurs in the last 2 ns of the Post (no AMP) trajectory. As C74 twists away from its original binding site, it causes many of the crystal contacts between the CCA hairpin and GluRS to break. Due to the stochastic nature of this transition and the time window of the network analysis, the Post (no AMP) state was caught before these contacts were broken. The Post (no AMP/GluNH$_2$) state shows especially low numbers of contacts with the acceptor stem and CCA hairpin as well as high numbers of contacts with the D and anticodon arms.

Change in interface contacts during tRNA dissociation

To examine the interface changes caused by tRNA dissociation, the interaction energy differences were calculated between the Pre-transfer and Post (no AMP/GluNH$_2$) states (see Figures **??**b). Further results for the Post (H-AMP) and Post (AMP) states are found in Supplementary Figure **??**. The Post (no AMP/GluNH$_2$) state has many interface interactions, particularly in the CD and the 4HJ, which weaken as the CCA hairpin dissociates from the GluRS active site. The main exception is at the 4HJ where the helix containing Lys316 and Arg319 shifts its position slightly closer to the tRNA, allowing it to make stronger interactions with A24 and C25. This also moves the loop containing Glu320, bringing it closer to the D stem phosphate backbone. There is little difference in the ACB domain which remains bound to the anticodon even as the CCA end undocks.

The Post (H-AMP) state shows minimal differences from the Pre-transfer state other than three residues in the C-terminal half of the Rossman fold. Four attractive residues (Arg163, Lys180, Lys241, and Lys426) have moved closer and three (Arg147, Lys243, and Lys382) have moved further away. This agrees with the other analyses that show the Post (H-AMP) state to be slightly more stable than the Pre-transfer state. In the Post (AMP) state, several attractive interface interactions weaken and repulsive contacts strengthen along the interface, with the exception of the anticodon binding domain. This agrees with the network and free energy analyses showing the Post (AMP) state to be one of the closest to dissociation.

Tables

Table S1: Number of network contacts for edges connecting $tRNA^{Glu}$ to GluRS. Each pair of values is given for a region of $tRNA^{Glu}$, and values were calculated across the last 5 ns of the 20 ns trajectories. Here, "AS" refers to the base paired portion of the acceptor stem, and nucleotides 73–76 are denoted "ACCA."

Table S2: Important GluRS residues interacting with $tRNA^{Glu}$ identity elements. The identity elements are grouped as in the network analysis. The residues were selected from those identified in the local energetics analysis to make highly energetic contacts with the tRNA. The parts of the nucleotide and residue forming the direct contacts are denoted in parenthesis with the following abbreviations (bb = phosphate backbone, rib = ribose, sc = sidechain). The residues within 5 Å were selected from the crystal structure and end of the Post (no AMP/$GluNH_2$) simulation (20 ns).

Table S3: Detailed MM-PBSA binding free energy values for the Pre-transfer state. The first set of columns show the values resulting in $\langle \Delta G_{adenylate} \rangle$ of -39.15 kcal/mol. The second set correspond to $\langle \Delta G_{tRNA} \rangle$. The 95% confidence interval range for each quantity is ± the value shown in parentheses.

Table S4: MM-PBSA free energy differences for tRNA binding in kcal/mol for alternative system states containing AMP. The 95 % confidence interval range for each value is ± the number shown below in parentheses. Standard deviations for the $\langle \Delta G_{binding} \rangle$ were 17-24 kcal/mol.

Table S5: List of organisms in the QR set for D-GluRS and $tRNA^{Glu}$

Figures

Figure S1: Comparison of the active site between the crystal structure and the equilibrated Pre-transfer state. Distances are measured between the heavy atoms with the black values from the crystal structure and the blue values are averages over the last 16 ns of the 20 ns Pre-transfer trajectory. Atoms and bonds in blue are unique to the trajectory. The CH_2 in the analog and a water from the crystal structure are colored red for clarity. Circled "W"'s indicate regions of high water density with gray bonds indicating waters mediating contacts.

Figure S2: Motion of tRNA over 80 ns in the Post (no AMP/GluNH_2) state. The tRNA and charging amino acid are shown at four evenly distributed timepoints along the trajectory. Each frame was aligned to the crystal structure by the protein.

Figure S3: tRNA motion in the active site. The distance between the α–amino group on the charging amino acid to the Glu41 sidechain in the active site is shown as a function of time in the Pre-transfer, Post (H-AMP), and Post (no AMP/GluNH_2) states.

Figure S4: Residence of Mg^{2+} ions in two Pre-transfer states. The first run is shown by the tan tRNA, cyan protein, and green occupancy isosurfaces. The second run has black tRNA, blue GluRS, and red occupany isosurfaces. The isosurfaces mark locations occupied by resident ions.

Figure S5: Dynamical network of the Post (no AMP/$GluNH_2$) state. The shortest or optimal paths are shown between A76 and nucleotides C72 (green), U13 (blue), and C36 (red). Thicker edges indicate greater correlation between two nodes and the thickness of the path between Lys241 and

Figure S6: Mean non-bonded interaction energy difference for GluRS to $tRNA^{Glu}$ in the (a) Post (H-AMP), (b) Post (AMP), and (c) Post (no AMP/$GluNH_2$) states compared to the Pre-transfer state (atoms in the charging glutamate were not included). Residues that make attractive or repulsive interactions in the Pre-transfer state are shown in black or gray, respectively. Black peaks greater than zero represent residues moving further away from $tRNA^{Glu}$ while positive gray peaks correspond to residues moving closer in. The opposite is true for negative peaks. These values are averaged over the last 5 ns of the 20 ns trajectories.

Figure S7: Motion of tRNA in the absence and presence of EF-Tu. The tRNA and charging amino acid are shown in the Post (no AMP/$GluNH_2$) and Post (no AMP/EF-Tu) states after 50 ns of equilibration. The Post (no AMP/EF-Tu) simulation started out with an α–ammonium group on the charging glutamate moiety. At 10 ns, this group was deprotonated, allowing the CCA end to undock from GluRS, and at 30 ns the α–amino group was reprotonated since it was surrounded by solvent. The equilibrated structures were aligned to the crystal structures of GluRS and EF-Tu (see Methods) by the protein backbones. The initial position of the charging amino acid in GluRS is shown in red, the position after 50 ns in the absence or presence of EF-Tu in white and purple respectively, and the position docked in the EF-Tu (crystal structure) in blue (final).

Supplementary Tables

Source	Pre-transfer	Post (H-AMP)	Post (AMP)	Post (no AMP)	Post (no AMP/GluNH$_2$)
ACCA	20	21	15	22	6
AS	25	20	18	18	18
Core	26	21	19	18	24
AC	22	22	20	16	24
Total	93	84	72	74	72

Table 5:

Identity Element	Residues forming direct contacts	Residues within 5 Å
Pre-transfer		
G1	none	none
C72	none	Glu172
G2	none	Glu172
U71	Lys243 (bb/sc)	Glu208
C4	none	none
G69	Arg237 (rib/sc) Lys243 (rib/bb)	Glu207 Lys241
U11	none	Lys241 Lys309
A24	Glu282 (rib/sc) Lys309 (rib/sc)	none
C12	Glu282 (rib/sc) Lys309 (rib/sc)	none
G23	Glu282 (base/sc)	Lys309
C9	none	none
U13	none	Arg297
G22	none	none
A46	none	none
C34	Arg417 (bb/sc) Arg435 (base/sc)	none
U35	none	Arg358 Arg435 Glu443
C36	Arg358 (base/sc)	Glu443
A37	none	Arg311 Arg319 Arg358 Glu443
Post (no AMP/GluNH_2)		
G1	none	none
C72	Arg116 (rib/sc)	none
G2	Glu172 (rib/sc)	none
U71	none	none
C4	none	none
G69	Glu207 (base/sc) Arg237 (rib/sc)	Lys241 Lys243
U11	Lys241 (bb/sc)	Lys309
A24	Glu282 (rib/sc) Lys309 (rib/sc)	none
C12	none	Lys309
G23	none	Lys309
C9	none	none
U13	none	none
G22	none	none
A46	none	none
C34	Arg417 (bb/sc) Arg435 (base/sc)	none
U35	none	Arg358 Arg435 Glu443
C36	Arg358 (base/sc)	Glu443
A37	none	Arg319 Arg358

Table 6:

Pre-transfer	Complex	GluRS/tRNA	Adenylate	Difference	Complex	GluRS/Adenylate	tRNA	Difference
$\langle E_{VdW} \rangle$	-2041.96	-2013.15	12.54	-41.34	-2041.96	-1996.16	198.69	-244.49
	(1.86)	(1.83)	(0.12)	(0.20)	(1.86)	(1.45)	(1.20)	(0.34)
$\langle E_{elec} \rangle$	-235075.29	-233086.62	-1984.77	-3.90	4560.52	-16559.16	21861.89	-742.21
	(4.09)	(4.05)	(0.38)	(0.38)	(9.63)	(4.70)	(7.83)	(6.42)
$\langle E_{coulomb} + G_{polar} \rangle$	-41465.21	-40804.52	-173.61	-487.08	-235075.29	-140446.75	-94857.11	228.57
	(9.19)	(8.98)	(0.17)	(0.50)	(4.09)	(2.91)	(2.69)	(0.74)
$\langle G_{non-polar} \rangle$	166.35	167.54	4.62	-5.81	166.35	121.71	73.71	-29.07
	(0.05)	(0.05)	(0.00)	(0.00)	(0.05)	(0.04)	(0.03)	(0.02)
$-T\Delta S$	-1242.30	-1238.00	-16.20	11.90	-1242.30	-968.70	-309.80	36.20
$\langle G_{binding} \rangle$	-234347.91	-232347.90	-1960.86	-39.15	-234347.91	-140590.98	-93748.14	-8.79
	(4.27)	(4.25)	(0.38)	(0.29)	(4.27)	(3.24)	(2.71)	(0.65)

Table 7:

	Post (AMP/H15h)	Post (AMP/GluNH$_2$/E41h)
$\langle \Delta E_{VdW} \rangle$	-237.11	-244.46
	(0.45)	(0.37)
$\langle \Delta E_{coulomb} + \Delta G_{polar} \rangle$	219.42	233.71
	(1.00)	(1.07)
$\langle \Delta G_{nonpolar} \rangle$	-30.67	-31.14
	(0.02)	(0.03)
-TΔS	37.10	37.80
$\langle \Delta G_{binding} \rangle$	-11.26	-4.10
	(0.77)	(1.03)

Table 8:

Species	D-GluRS	tRNA CUC	tRNA UUC
Aquifex aeolicus			1
Acaryochloris marina			1
Acidobacteria bacterium	1		
Aeromonas hydrophila			1
Anaeromyxobacter sp.			1
Arcobacter butzleri			1
Arthrobacter aurescens	1		
Atopobium rimae	1		
Bacillus thuringiensis			1
Bacteroides uniformis		1	
Bacillus subtilis			1
Blastopirellula marina	1		
Brucella melitensis			1
Campylobacter curvus		1	
Campylobacter fetus		1	
Candidatus Carsonella ruddii			1
Candidatus Liberibacter	1		
Candidatus Pelagibacter ubique			1
Candidatus Ruthia magnifica			1
Candidatus Sulcia muelleri			1
Candidatus Vesicomyosocius okutanii			1
Chlamydia muridarum	1		
Clostridium hiranonis	1		
Clostridium sp.		1	
Clostridium tetani	1	1	
Cyanothece sp.			1
Deinococcus radiodurans	1		
Desulfatibacillum alkenivorans			1
Ehrlichia canis			1
Escherichia coli			1
Eubacterium dolichum			1
Flavobacteriales bacterium			1
Gloeobacter violaceus	1		
Hahella chejuensis			1
Heliobacterium modesticaldum	1		
Herpetosiphon aurantiacus	1		
Hyphomonas neptunium	1		
Kordia algicida		1	
Lactobacillus brevis		1	
Lactobacillus delbrueckii		1	
Lactobacillus johnsonii			2
Legionella pneumophila	1		
Leuconostoc mesenteroides		1	
Methylibium petroleiphilum			1
Microscilla marina	1		2
Mycoplasma mycoides			1
Mycoplasma penetrans			1
Mycoplasma pulmonis			1
Nostoc punctiforme			1
Oceanospirillum sp.	1		
Opitutaceae bacterium		1	
Petrotoga mobilis		1	1
Planctomyces maris			1
Plesiocystis pacifica		2	
Propionibacterium acnes	1	1	
Prosthecochloris vibrioformis	1		
Pseudoalteromonas haloplanktis			1
Psychroflexus torquis	1	1	
Rhizobium leguminosarum		1	
Rhodopirellula baltica			1
Ruminococcus gnavus			1
Ruminococcus obeum		1	
Sphingomonas sp.	1		
Stigmatella aurantiaca	1		
Streptococcus pneumoniae			1
Thermotoga maritima	1		
Thermus thermophilus	1	1	
Thiomicrospira denitrificans			1
Treponema pallidum	1		
Victivallis vadensis			1
Wolinella succinogenes			1

Table 9:

Supplementary Material (To be Published) - Figure11

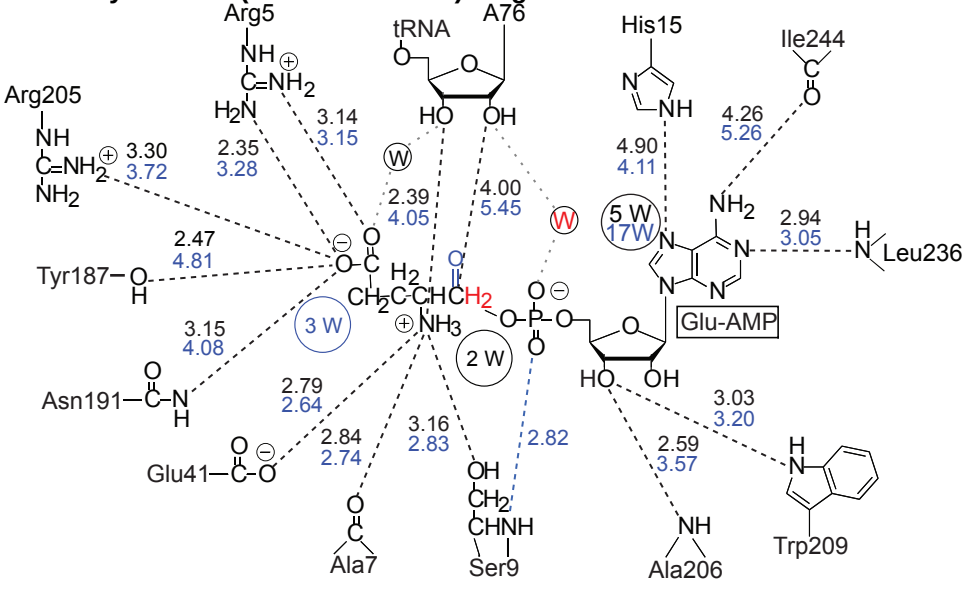

Supplementary Material (To be Published) - Figure12

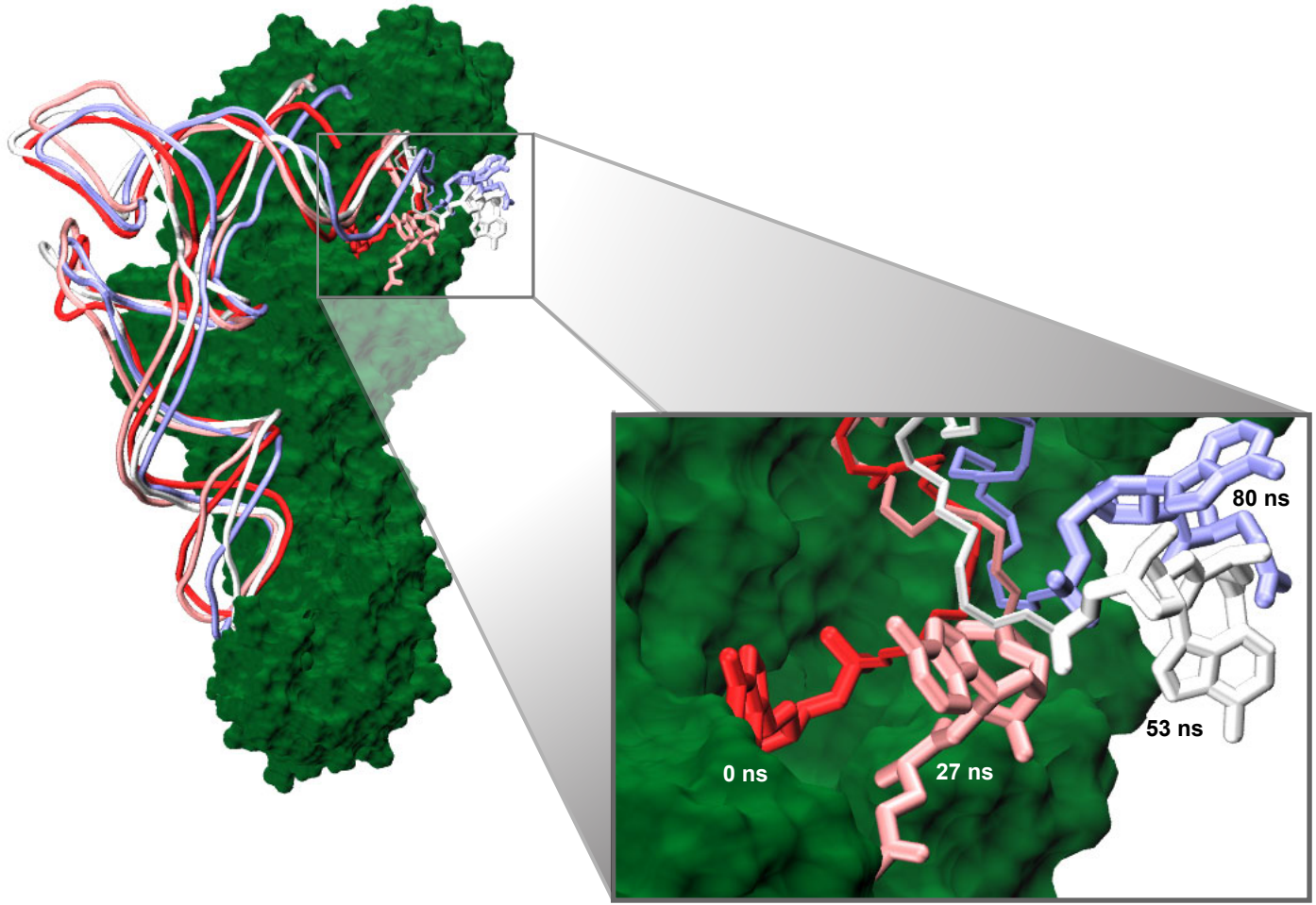

Supplementary Material (To be Published) - Figure13

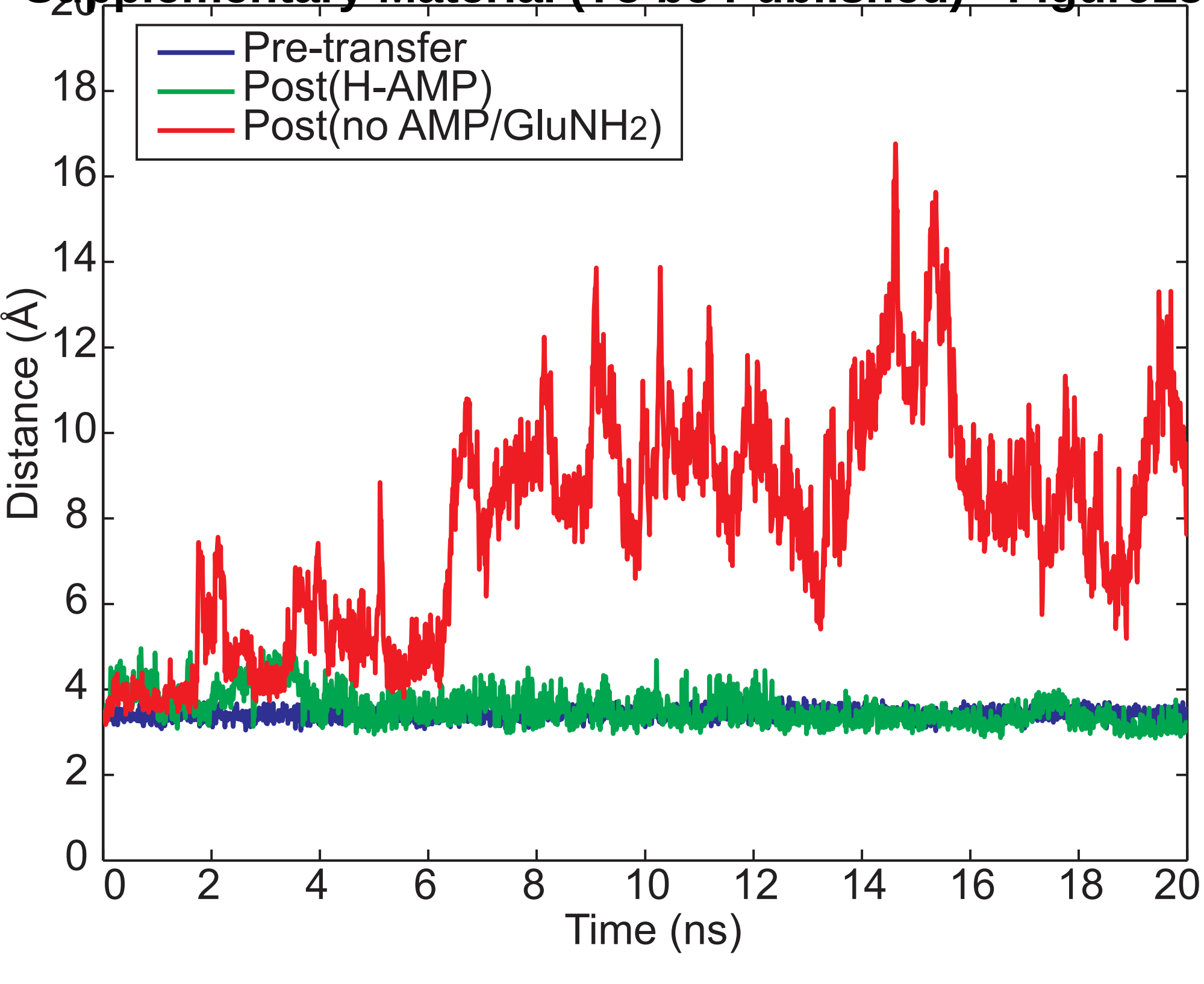

Supplementary Material (To be Published) - Figure14

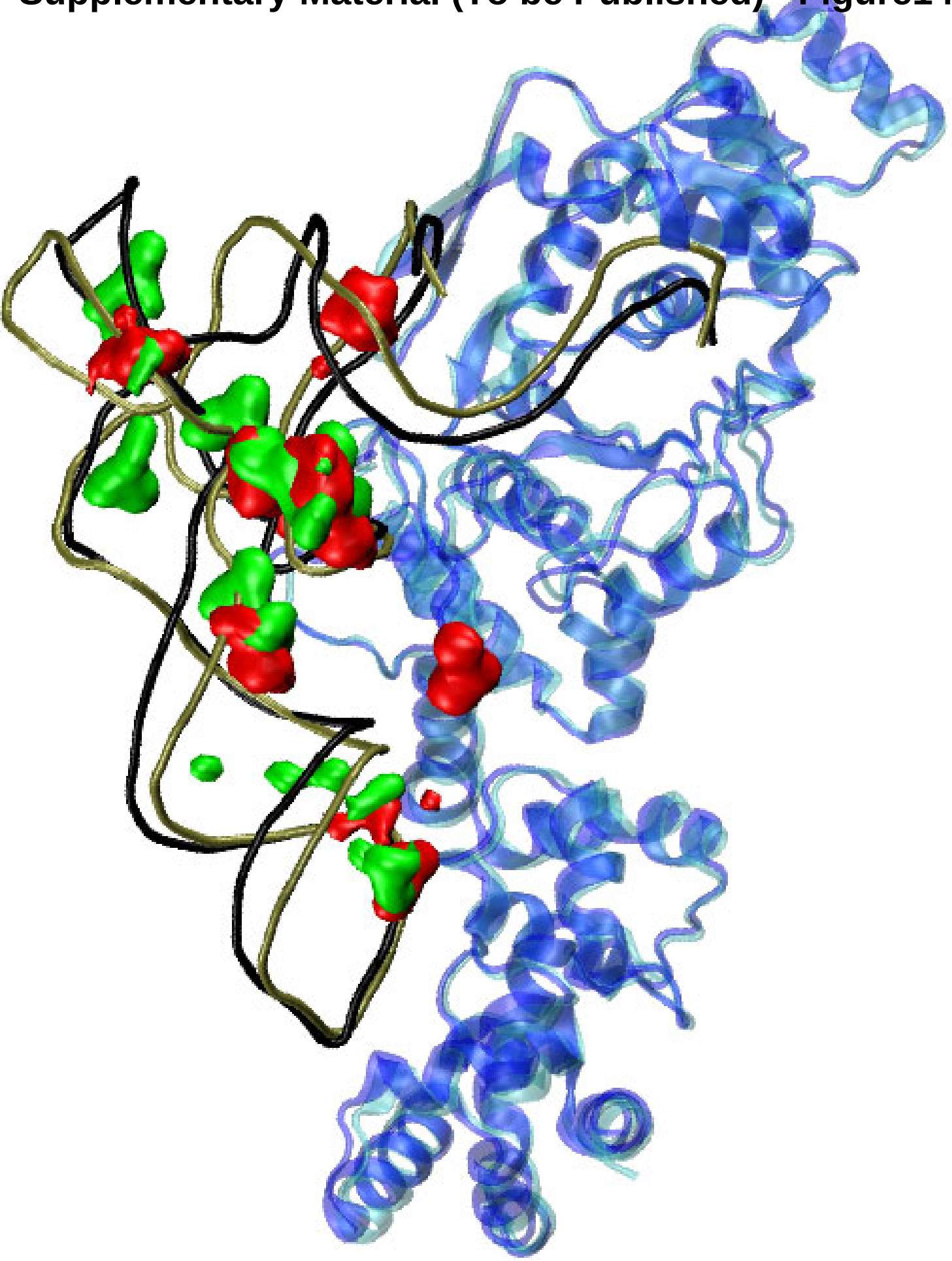

Supplementary Material (To be Published) - Figure15

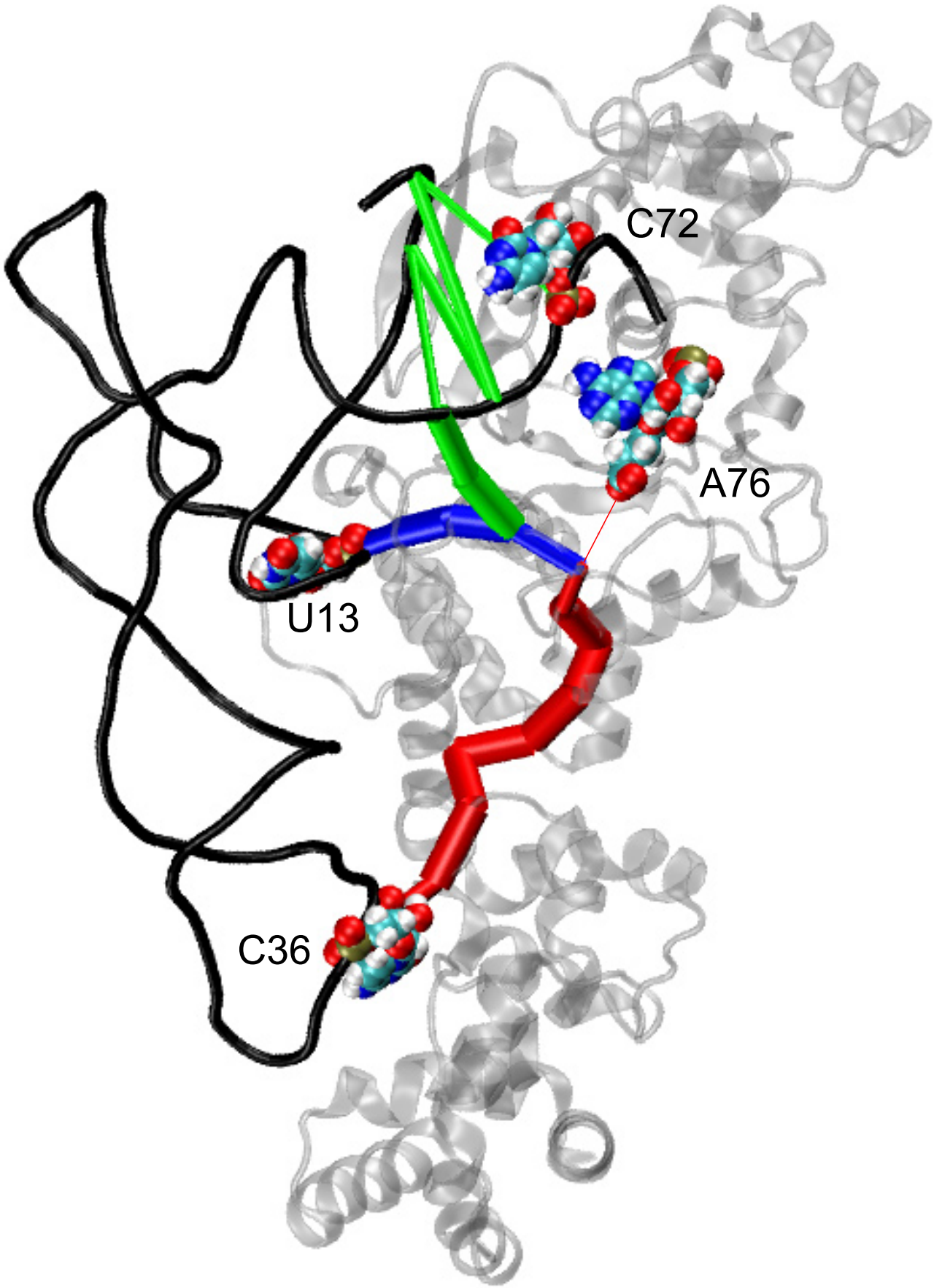

Supplementary Material (To be Published) - Figure16

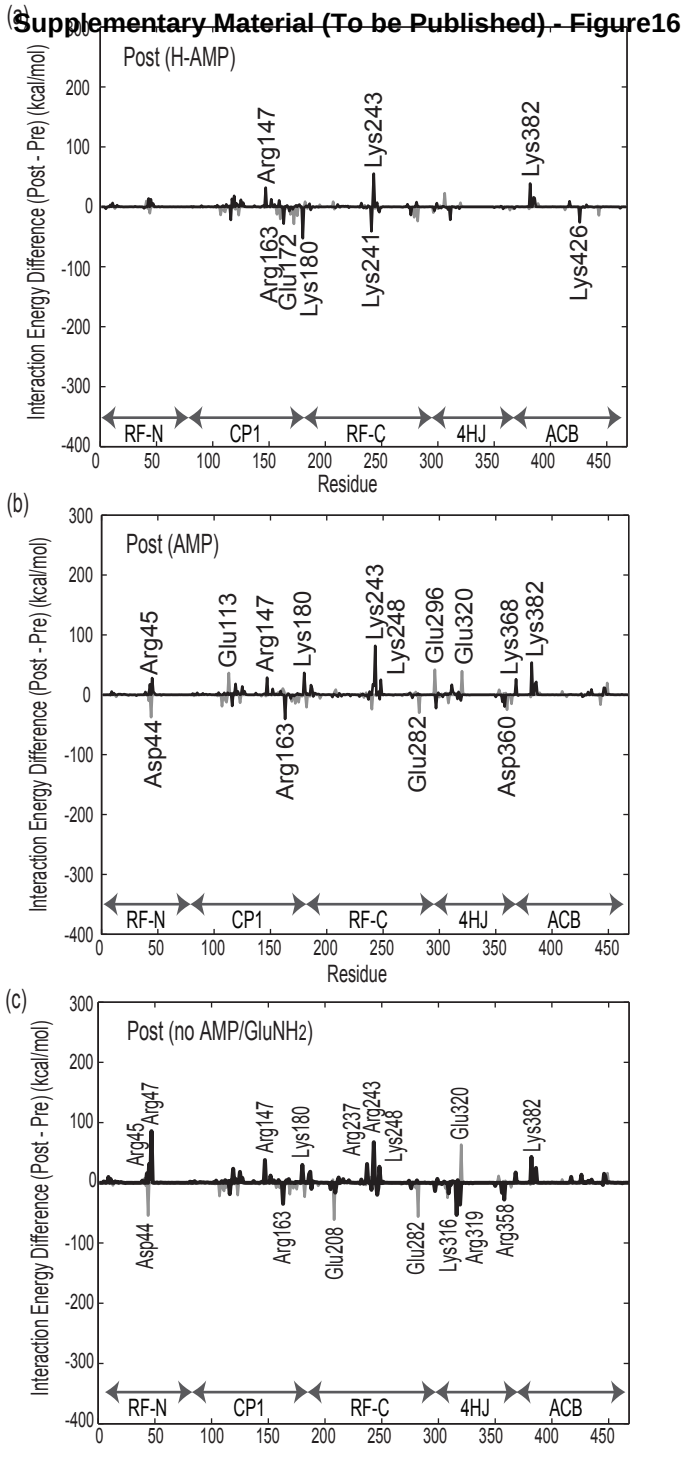

Supplementary Material (To be Published) - Figure17